

Electronic Supporting Information

Functionalisation of gold nanoparticles with ruthenium(II) polypyridyl complexes for their application in cellular imaging

Sandra Estalayo-Adrián,^{*ab} Gavin J. McManus,^c Hannah L. Dalton,^a Aramballi J. Savyasachi,^a John M. Kelly^a and Thorfinnur Gunnlaugsson^{*a}

^aSchool of Chemistry and Trinity Biomedical Sciences Institute (TBSI), Trinity College Dublin, The University of Dublin, Dublin 2, Ireland. E-mail: estalays@tcd.ie, gunnlaut@tcd.ie

^bAdvanced Materials and BioEngineering Research (AMBER) Centre, Trinity College Dublin, The University of Dublin, Dublin 2, Ireland

^cSchool of Biochemistry and Immunology, Trinity Biomedical Sciences Institute (TBSI), Trinity College Dublin, The University of Dublin, Dublin 2, Ireland

Table of Contents	Page No
Fig. S1. ¹ H NMR spectrum of 3	S2
Fig. S2. ¹³ C NMR spectrum of 3	S3
Fig. S3. FTIR spectrum of 3	S3
Fig. S4. ¹ H NMR spectrum of 1	S4
Fig. S5. ¹³ C NMR spectrum of 1	S5
Fig. S6. FTIR spectrum of 1	S5
Fig. S7. ESI ⁺ -HRMS spectrum of 1	S6
Fig. S8. ¹ H NMR spectrum of 2	S6
Fig. S9. ¹³ C NMR spectrum of 2	S7
Fig. S10. FTIR spectrum of 2	S7
Fig. S11. MALDI ⁺ -HRMS spectrum of 2	S8
Fig. S12. UV-vis absorption, excitation and emission spectra of 1 , 2 , 1·AuNP and 2·AuNP	S8
Fig. S13. Confocal fluorescence microscopy images of HeLa cells treated with 1	S9
Fig. S14. Bright field images of HeLa cells treated with 1·AuNP and 2·AuNP	S9
Fig. S15. Toxicity profiles of 1 and 2 in HeLa cells	S10

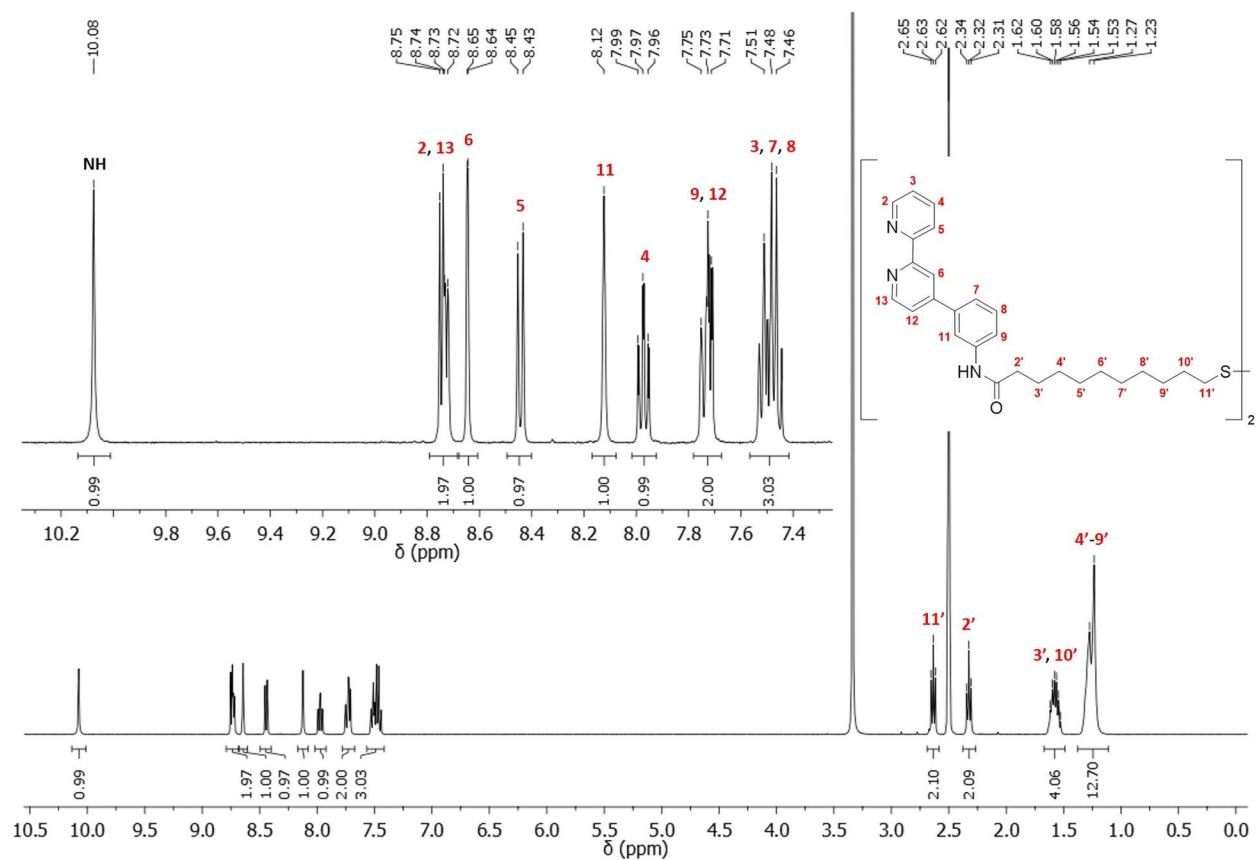


Fig. S1. ^1H NMR (400 MHz, $\text{DMSO-}d_6$) spectrum of ligand **3**.

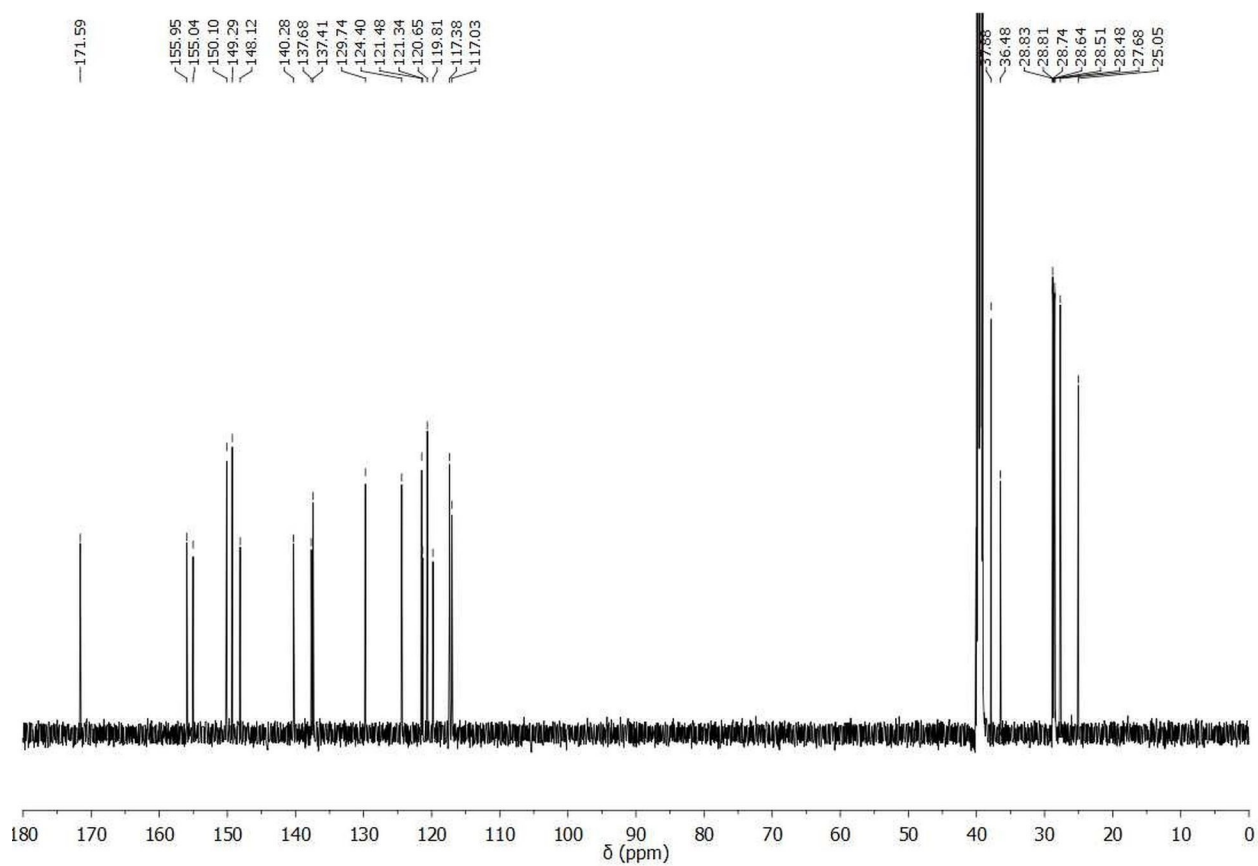


Fig. S2. ^{13}C NMR (101 MHz, $\text{DMSO-}d_6$) spectrum of ligand **3**.

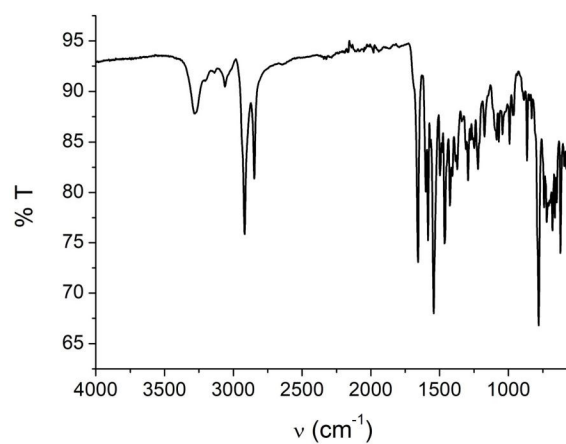


Fig. S3. FTIR spectrum of ligand **3**.

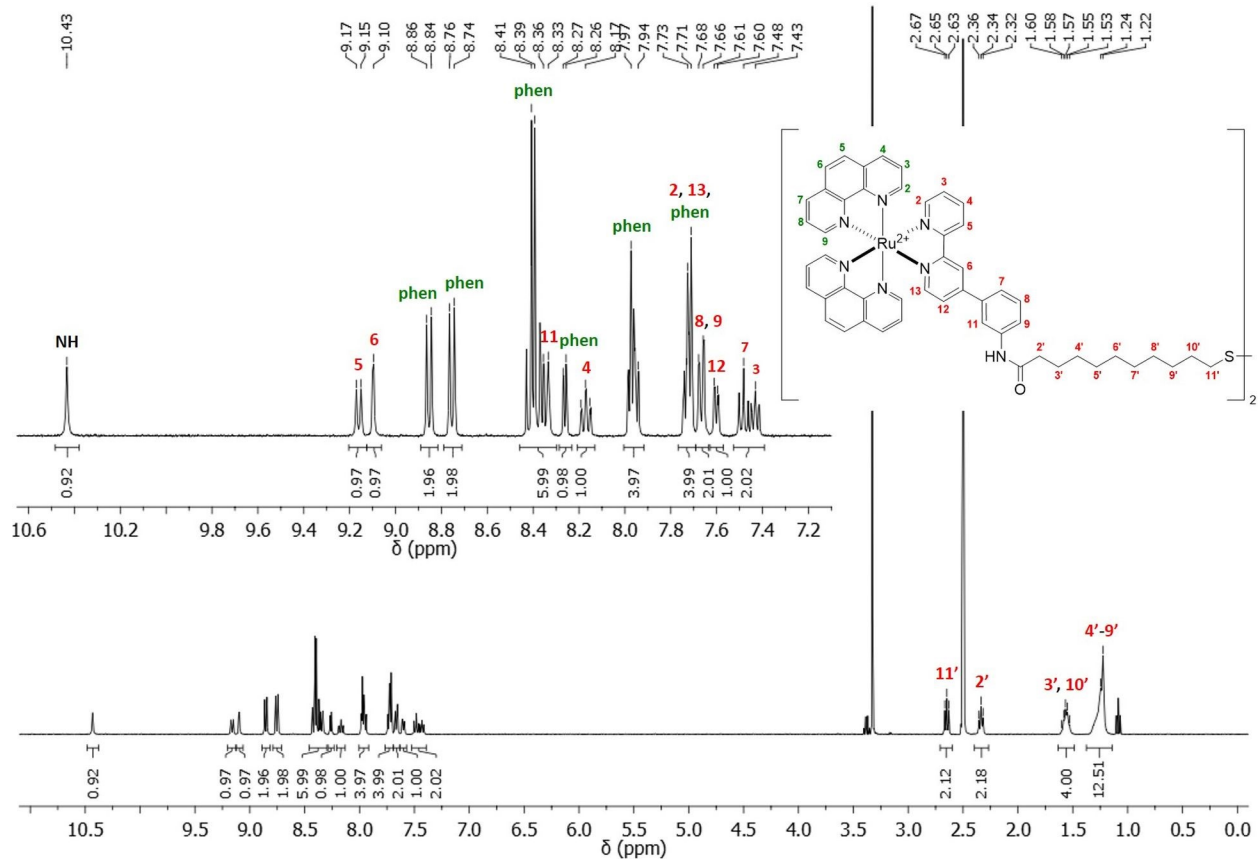


Fig. S4. ^1H NMR (400 MHz, DMSO- d_6) spectrum of complex **1**. Signals corresponding to phen ligands are in green and signals assigned to ligand **3** are in red.

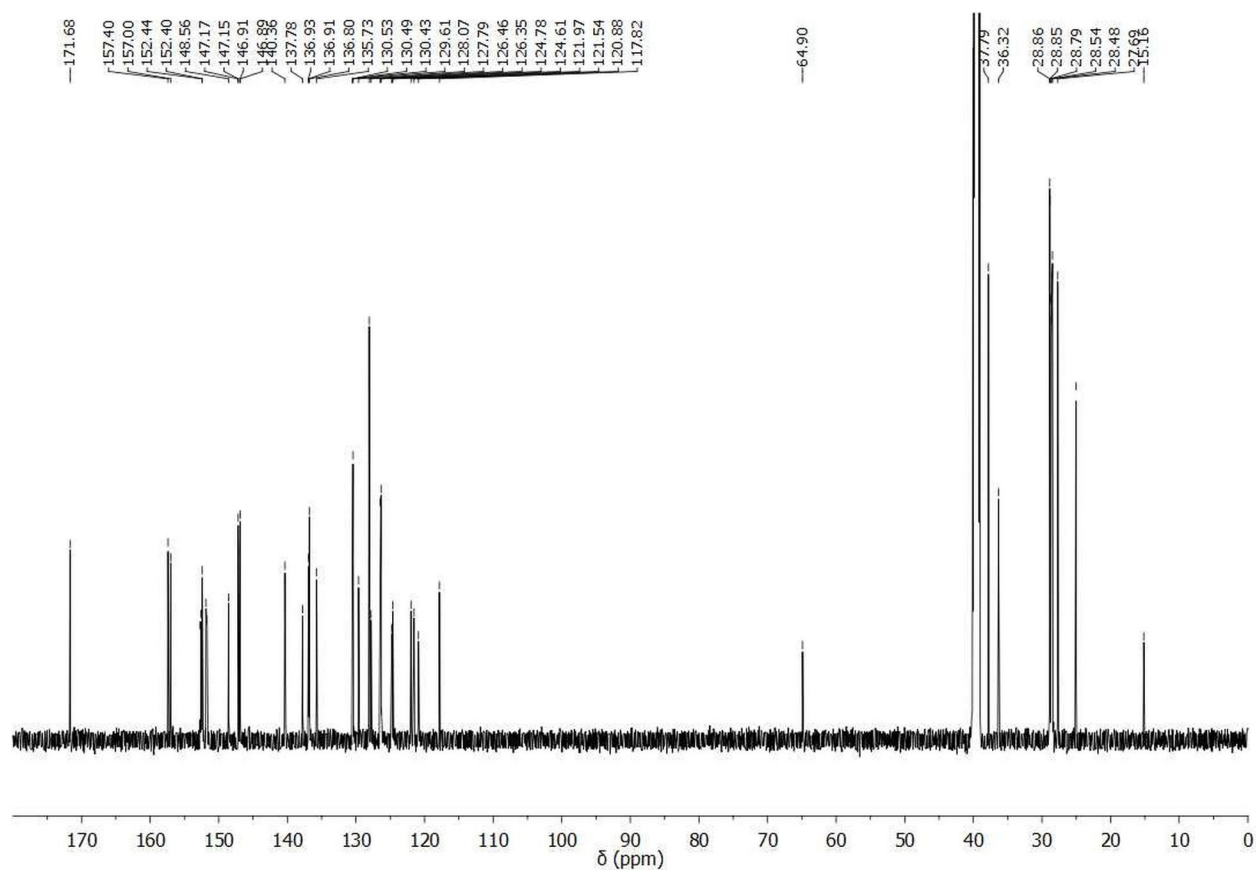


Fig. S5. ^{13}C NMR (101 MHz, $\text{DMSO-}d_6$) spectrum of complex **1**.

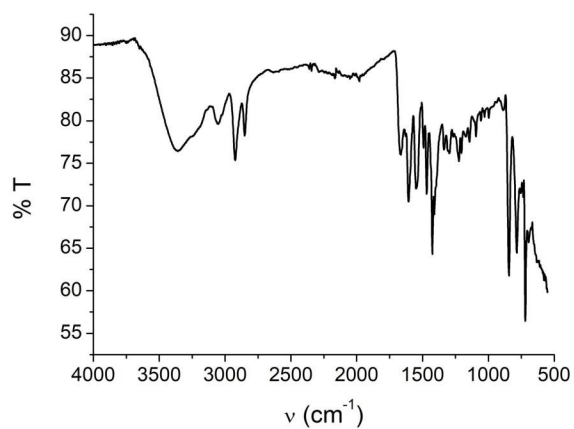


Fig. S6. FTIR spectrum of complex **1**.

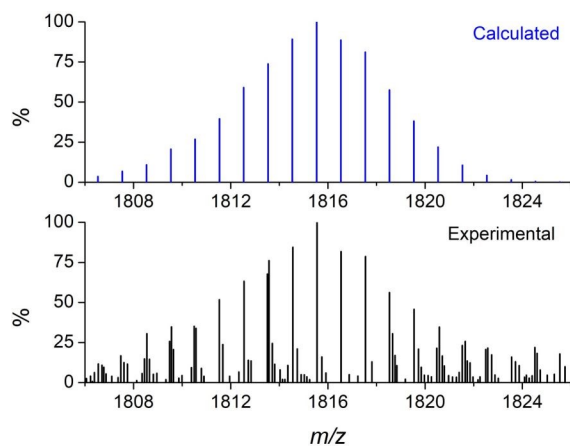


Fig. S7. Comparison between the calculated (blue) and experimental (black) isotopic distribution pattern for complex **1** from matrix-assisted laser desorption/ionisation (positive mode) high resolution mass spectrometry analysis.

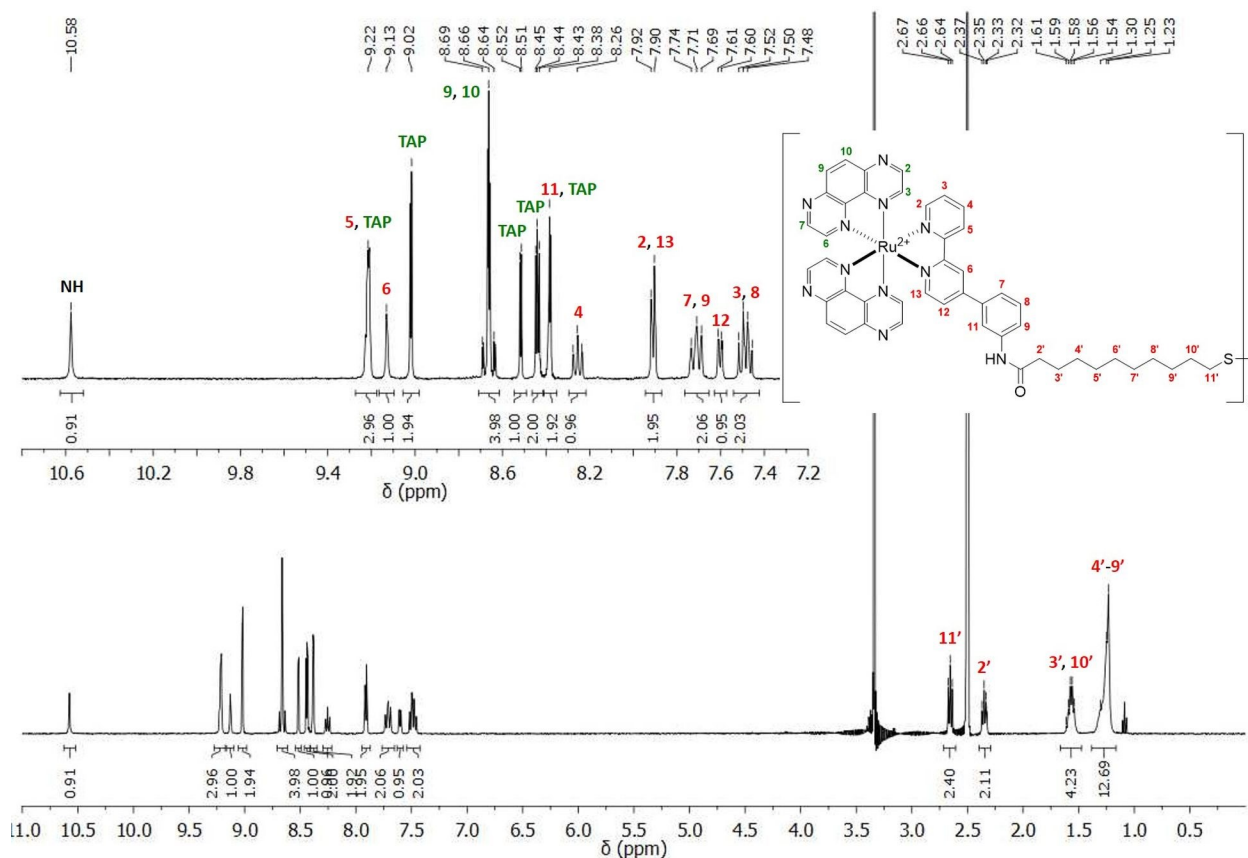


Fig. S8. ^1H NMR (400 MHz, $\text{DMSO-}d_6$) spectrum of complex **2**. Signals corresponding to TAP ligands are in green and signals assigned to ligand **3** are in red.

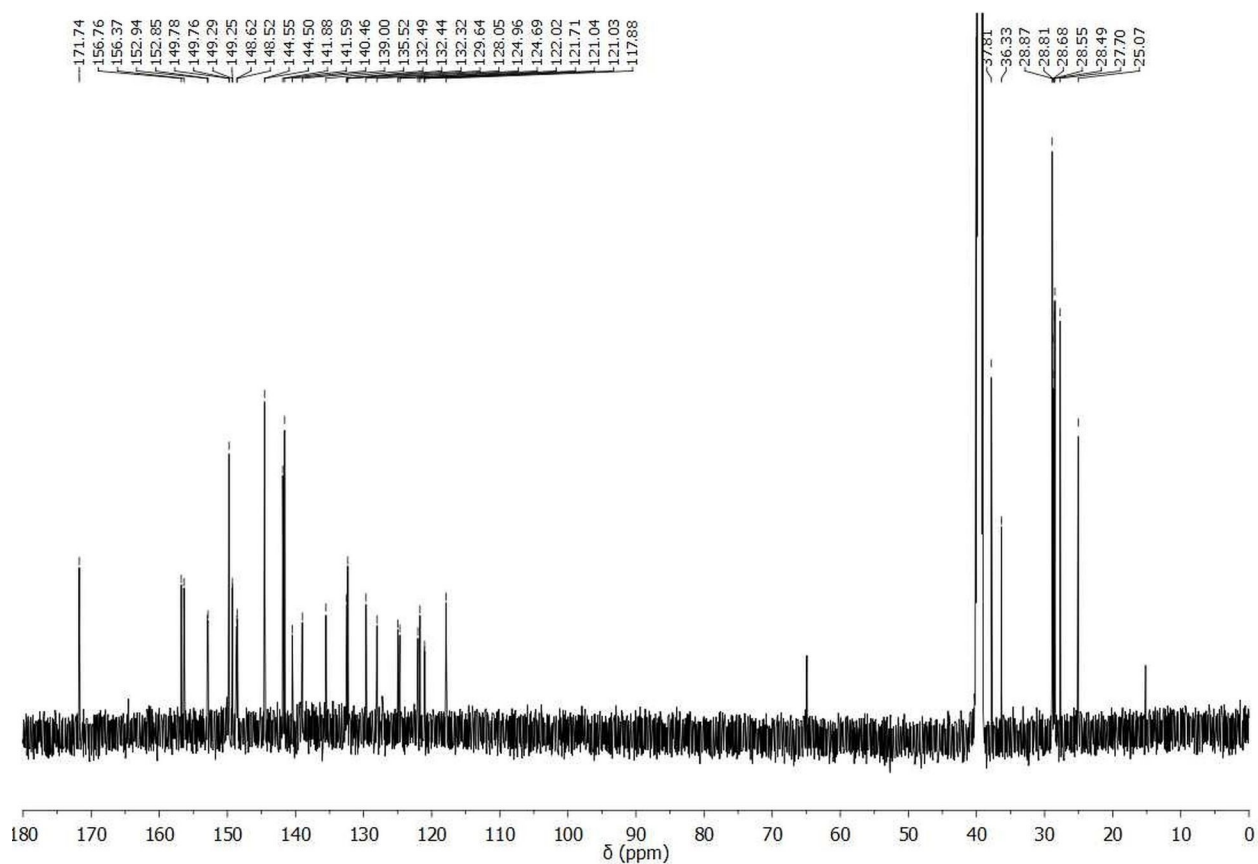


Fig. S9. ^{13}C NMR (101 MHz, $\text{DMSO-}d_6$) spectrum of complex **2**.

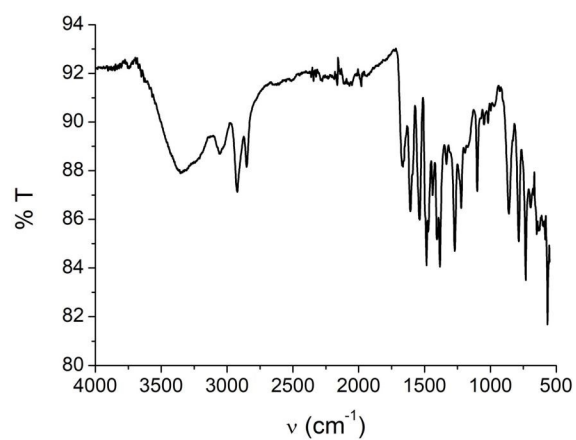


Fig. S10. FTIR spectrum of complex **2**.

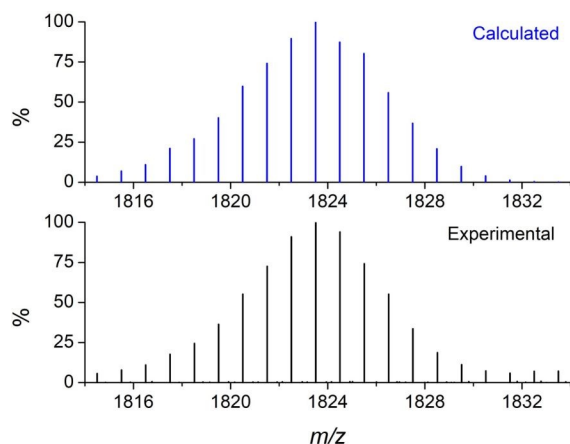


Fig. S11. Comparison between the calculated (blue) and experimental (black) isotopic distribution pattern for complex **2** from matrix-assisted laser desorption/ionisation (positive mode) high resolution mass spectrometry analysis.

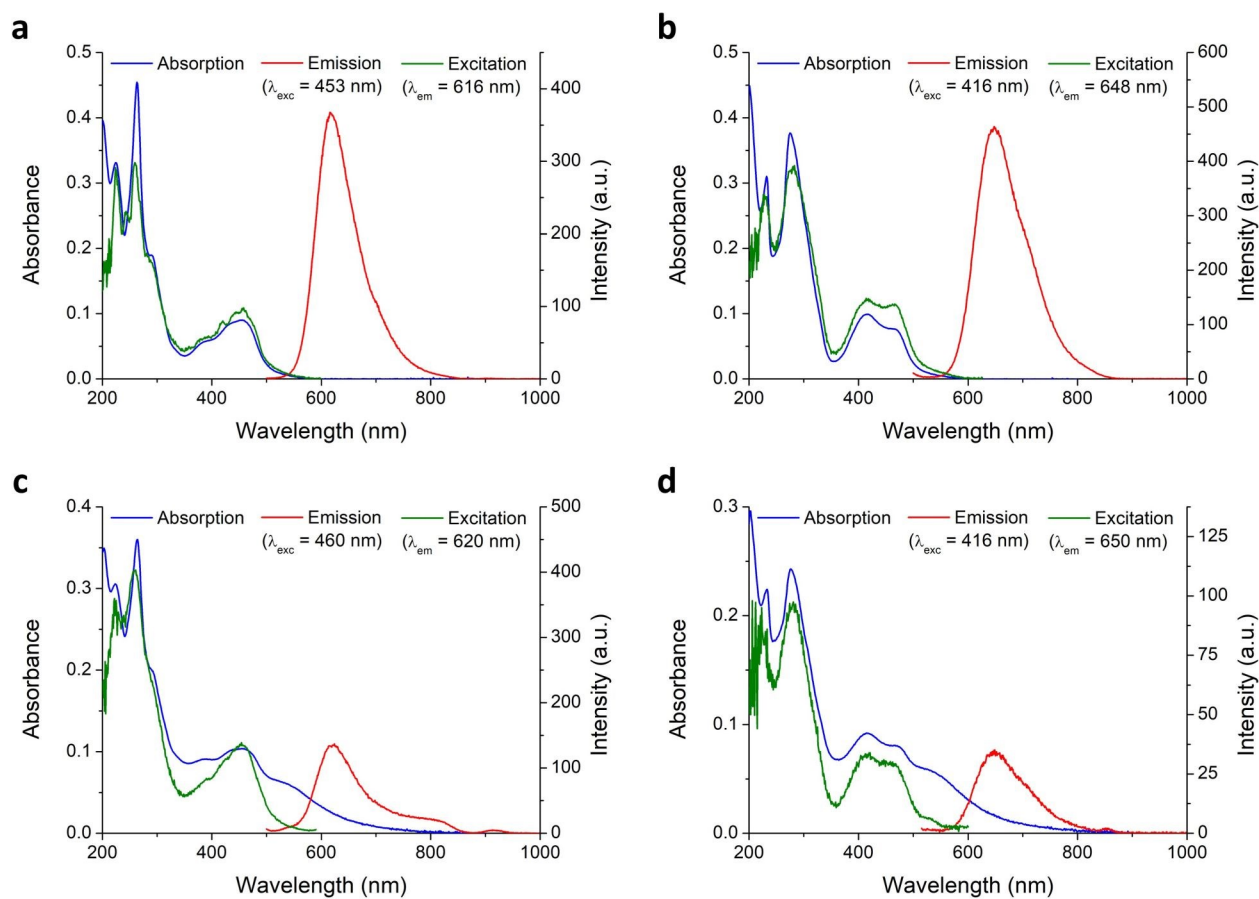


Fig. S12. UV-vis absorption, excitation and emission spectra of (a) **1**, (b) **2**, (c) **1·AuNP** and (d) **2·AuNP** in 10 mM sodium phosphate-buffered aqueous solution at pH 7.4, at 298 K.

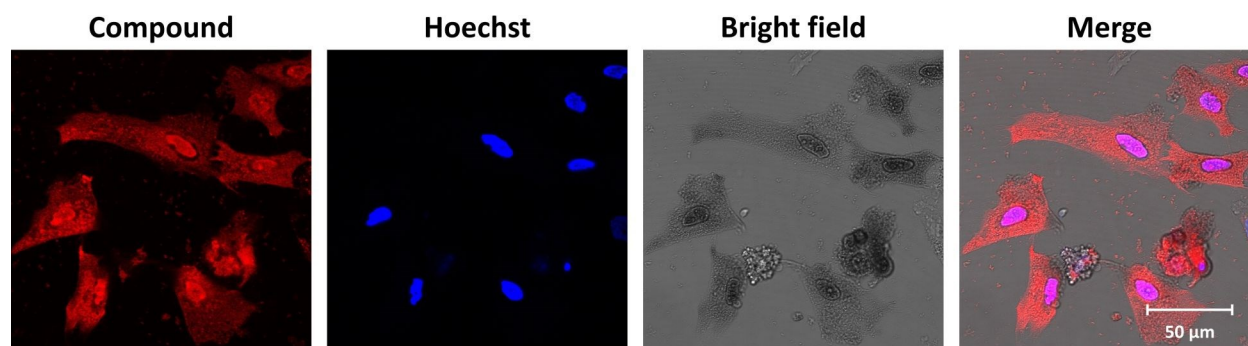


Fig. S13. Confocal fluorescence microscopy images of HeLa cells showing the nuclear uptake of **1** (red) at 20 μM after 24 h incubation. The nucleus is stained blue with Hoechst 33258.

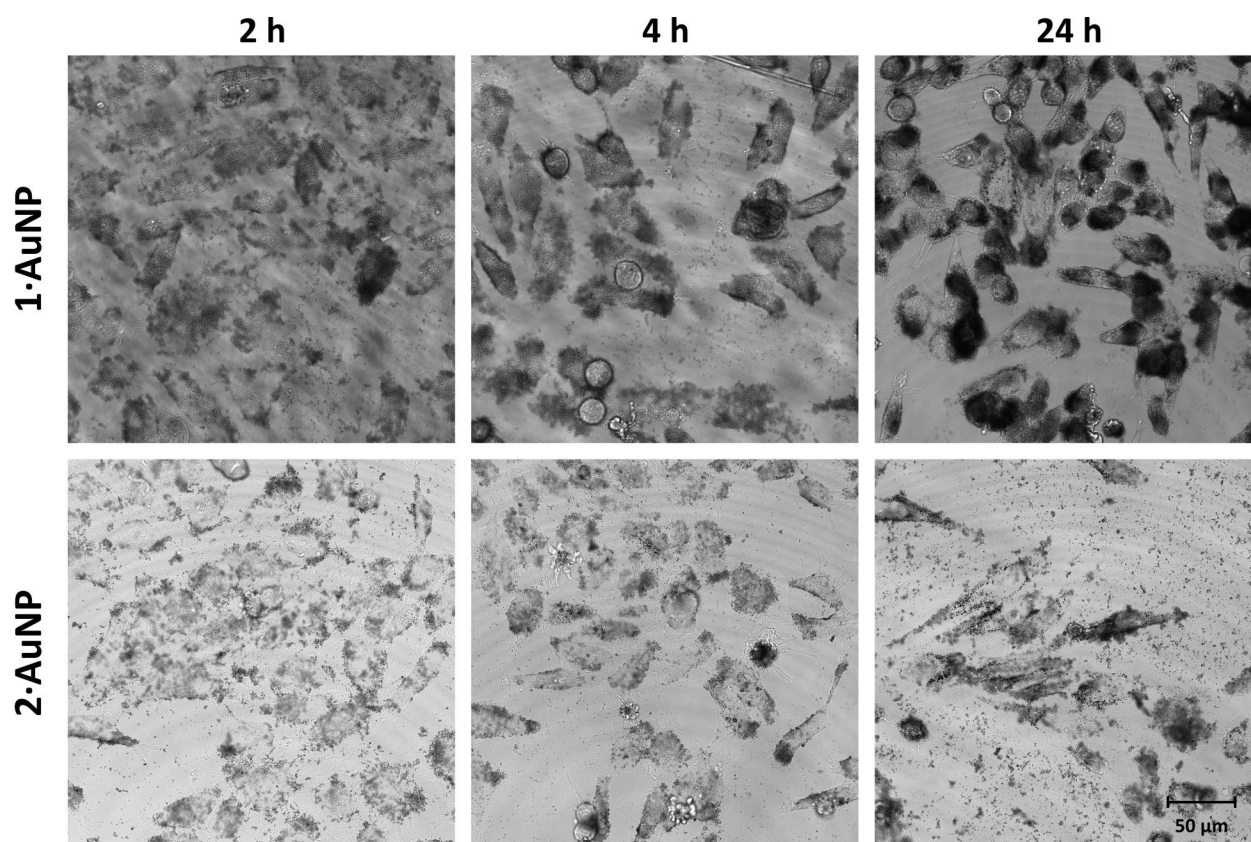


Fig. S14. Bright field images of HeLa cells showing the uptake of **1·AuNP** and **2·AuNP** at *ca.* 20 μM Ru(II) complex concentration after 2, 4 and 24 h incubation.

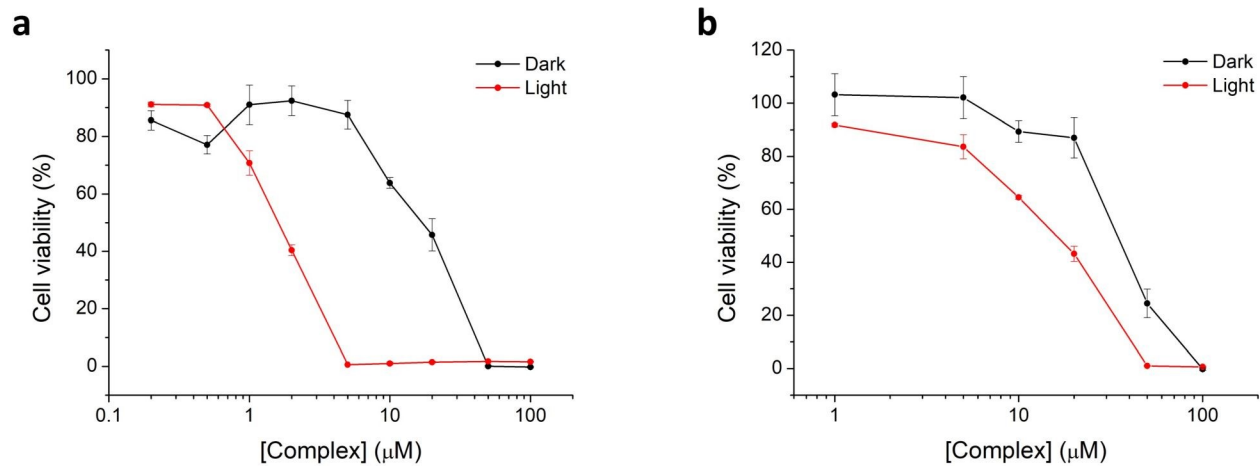


Fig. S15. Toxicity profiles of (a) **1** and (b) **2** in HeLa cells.